Anal. Bioanal. Electrochem., Vol. 14, No. 11, 2022, 1027-1043

Analytical & Bioanalytical Electrochemistry

2022 by CEE
www.abechem.com

Full Paper

Calibration Curve Approaches for Nonlinear Data Points Obtained in Colo 320 Exosomes Determination

Sevda Akay Sazaklioglu,[1,2] Hilal Torul,[3] Hilal Kabadayi,[4] Hafize Seda Vatansever,[4,5] Ugur Tamer,[3] and Huseyin Celikkan[6,*]

[1]*Department of Medical Services and Techniques, Ankara Medipol University, 06050, Ankara, Turkey*
[2]*Graduate School of Natural and Applied Science, Gazi University, 06560, Ankara, Turkey*
[3]*Faculty of Pharmacy, Department of Analytical Chemistry, Gazi University, 06330, Ankara, Turkey*
[4]*Department of Histology and Embryology, Manisa Celal Bayar University, 45030, Manisa, Turkey*
[5]*DESAM Institute, Near East University, Mersin 10, Turkey*
[6]*Faculty of Science, Department of Chemistry, Gazi University, 06560, Ankara, Turkey*

*Corresponding Author, Tel.: + 905335512852
E-Mail: celikkan@gazi.edu.tr

Received: 1 September 2022 / Received in revised form: 17 November 2022 / Accepted: 23 November 2022 / Published online: 30 November 2022

Abstract- The limit of detection (LOD) is defined as the lowest quantity or concentration of a component that can be reliably distinguished from the limit of blank (LOB). LOD value is one of the most important parameters considered for many determination methods and is usually calculated on the linear correlation between signal and concentration. However, the linear correlation may not always be obtained in experimental studies. We claim that data with low linear correlation have meaning, and we present such a study because analytical studies based on these data are not easily understood in the literature. In this manuscript, we suggest that a calibration curve can be obtained from nonlinear data points and the LOD value can be calculated. We tested this approach for the determination of exosomes and supported it with mathematical calculations. We produced a label-free sensor using anti-CD63 on the gold electrode for selective and reliable impedimetric detection of the exosomes obtained from Colo 320 cell lines in data points that are high concentrations and out of linearity. We characterized in detail what each calculation means. This sensor with a LOD value of 3.90×10^{11} exosome particles μL^{-1} and with a cubic polynomial model for the calibration curve was considered sensitive and reliable, especially for high vesicle content of samples such as cell culture medium.

Keywords- Nonlinear calibration curve; Exosome determination; Electrochemical impedance spectroscopy; Mathematical models, Biosensors

1. INTRODUCTION

Exosomes are sub-micron-sized lipid transporters released from cells by exocytosis. The diameter of an exosome of endosomal origin ranges from 40 to 160 nm (average ~100 nm). Transmembrane proteins such as the tetraspanins CD9, CD63, CD81, and CD82 are widely used to identify exosomes [1]. It is possible to list many methods for separating exosomes from extracellular vesicles of different sizes and masses. One of the most common techniques is ultracentrifugation which requires centrifugation steps up to 200,000 g [2]. Recently, some researchers have used kit isolation due to its ease of application [3]. Another recent method for isolation is immunoaffinity-based methods, which are more effective in terms of specificity, affinity, and stability in the isolation of exosomes.

Exosomes have a great effect on striking issues such as intercellular communication, and immune response, and are a cancer marker, considering the functions of exosomes. Exosomes play a critical role in cell-to-cell communication by carrying out the transport processes of nucleic acids (DNA, mRNA, miRNA) [4], proteins, and lipids through cargo container cores [5]. The occurrence of the pickling process in lipid vesicles prevents the changes or deterioration of the cargo content. Furthermore, exosomes' uptake pathways or exosome specificity cause communication to proceed differently. For example, the macropinocytosis method suggests that the oncogenic signals induced by mutant KRAS expression lead to exosome uptake in human pancreatic cancer cells [6]. On the other hand, intercellular communication progresses more precisely during reproduction, pregnancy, and embryonic development processes. Exosomes are also involved in both infection prevention [7] and regulation of immune response [8]. For example, a relationship can be given between the exosomes in breast milk containing miRNA with immune functions and the exosome promoting healthy postnatal growth [9]. The studies to examine the intercellular communication process in normal and pathological cells have greatly increased the interest in exosomes. The most important reason for this is that factors known to be formed by cancer cells are released by exosomes [10] because exosomes affect neoplasia, tumor growth and metastasis, paraneoplastic syndromes, and resistance to therapy. In addition, the exosome level is high in blood samples of cancer patients (such as prostate, lung, and stomach) in healthy individuals [11,12].

In recent years, point of care assays-especially biosensors has attracted the attention of scientists in terms of the determination of exosomes due to their features such as ease of use, fast response, and high sensitivity [13]. Many biosensors have been developed, such as colorimetric [14,15], fluorescent [16,17], surface plasmon resonance (SPR) [18,19], surface-enhanced Raman scattering (SERS) [20] and electrochemical (EC) [21,22], biosensors. Electrochemical biosensors continue to be developed in terms of miniaturization and portability with the modernization of integrated circuit technology and the design of new electrode types. Electrochemical impedance spectroscopy (EIS) is a powerful technique for the characterization

of the sensor surface after modification as a method in which the resistance of the electrochemical interface is monitored.

The impedance of an electrochemical system is obtained in two ways: Nyquist and Bode plots. The Nyquist plot represents the real and imaginary parts (-ZIMAG vs. ZREAL) of the impedance at different frequencies and is used to explain the electrode surface with the equivalent circuit models such as the charge transfer resistance (RCT), double layer capacitance (CDL), etc. [23,24]. In the Bode plot, the diagram shows the impedance and phase angle against frequency (modulus [Ω] / phase [°] vs. frequency [Hz]) [25]. In the literature, the Randles equivalent circuit and its derivatives are used to obtain the RCT value as an output signal for impedimetric biosensors [26–28]. However, the Nyquist plot does not directly include impedance information via frequency. In Bode plots, magnitude and phase angle show how the magnitude of the impedance and the phase angle alter as a function of frequency [29]. Also, the Bode plot is based on the asymptotic approach that provides a simple method for plotting the logarithmic magnitude curve [30], and one can directly comment on the stability of the system, by using only one graph. In the Bode plot with its superior properties, the impedance overcomes the difficulty with the validation because of the nonlinearity in the calibration curve [31,32].

In the literature, there are many types of LOD calculation methods created with the signal points observed due to the presence of the analyte and are calculated by one of the methods in Table 1.

Table 1. Comparison of different methods for parameter "Detection limit"

Methods	Definitions	References
$\frac{S}{D} = \frac{2H}{h}$	H, the height of the peak; h, half-height width	[33]
$LOD = X_b + 3S_b$	X_b, the mean concentration of the blank; S_b, the standard deviation of the blank	[34]
$LOD = \bar{y}_0 + t \times S(y)$	$\bar{y}_0$, value of blank samples or 0;	[36]
$LOD = t \times S(x)$	S(x) is the standard deviation of the analyte; t, Student's Coefficient	[37]
$LOD = \bar{a} + t \times \frac{S_{(y)}}{\sqrt{n}}$	ā, average intercept; S(y) is standard deviation of blank samples; n, the number of repeated measurements	[38]
$LOD = 3.3 \times \frac{S_d}{m}$	m, the slope of the calibration function; Sd, standard deviation of the blank samples	[39]

Using the signal-to-noise method, the peak-to-peak noise around the retention time of the analyte is measured, and then the concentration of the analyte is estimated, which will give a signal equal to a certain value. The signal corresponding to the corresponding component is equal to 20 times the width h [33]. Blank analysis, on the other hand, is applied when the blank gives the result with a standard deviation other than zero [34]. For a linear calibration curve, the instrument response is assumed to be linearly related to concentration over a limited concentration range. It can be expressed in a model such as y=mx+n. In this method, a series of low values close to zero is used for the calibration curve, resulting in a more homogeneous distribution and a more relevant evaluation [35].

Method validation is an important requirement, especially in analytical determination processes. Although the most common is the one as linear calibration curves, applications for using this method on nonlinear curves are complex and not practical. Therefore, many different methods have been developed for nonlinear conditions in the literature. Zhou et al. proposed a nonlinear calibration method based on sinusoidal excitation and DFT transform. In that study, a mapping relationship was established between the sampling value and the theoretical calculation value, and the cubic spline interpolation method was used to further reduce the calibration error [40]. In addition, many different calibration curve methods have been developed in the literature, especially for highly concentrated biomolecules and curves that can be seen as exponential due to the logarithmic concentration axis [41–44].

In this work, we attached a specific antibody for the exosome surface antigen of CD63 by modifying the gold electrode (GE) surface and used the impedance data directly to obtain a calibration graph for exosome concentration. Four different mathematical models were obtained by using MATLAB software, and their standard deviations (SDs) and calibration coefficients (R^2) were analyzed. In addition, the R_{CT} values obtained by simulating the Nyquist plots and their appropriate equivalent circuit ($R_S(C_{DL}R_{CT})W$) were performed to show the linear relation in its calibration graph and to characterize the electrode surface. In this paper, we mainly aimed to explain the calculation of the limit of detection (LOD) in a nonlinear calibration curve proposed by more complex mathematical models comparing the ones already existing in the literature.

2. EXPERIMENTAL SECTION

2.1. Materials and reagents

11-Mercaptoundecanoic acid (MUA), 1-ethyl-3-(3-(dimethylamino)propyl) carbodiimide (EDC), N-hydroxysuccinimide (NHS), bovine serum albumin (BSA), potassium ferricyanide, potassium ferrocyanide were purchased from Sigma-Aldrich. Potassium dihydrogen phosphate, sodium hydrogen phosphate, sodium chloride, potassium chloride, and sodium hydroxide were purchased from Merck. All chemicals were of analytical grade and used without further purification. All aqueous solutions were prepared with deionized water of

resistivity not less than 18.2 MΩ (Millipore UHQ). An anti-CD63 antibody (clone MX-49.129.5) was purchased from Santa Cruz Biotechnology, Santa Cruz, CA, USA, and an anti-CD63 sample was used without further purification and diluted in pH 7.4 of PBS solution.

2.2. Apparatus

The electrochemical measurements were performed using IVIUM-CompactStat (Ivium Technologies, Netherlands) electrochemical analyzers. Gold electrode (2.0 mm diameter, Bioanalytical Systems, Inc.) after antibody modification was used as a working electrode. A Pt wire and Ag/AgCl electrode (Bioanalytical Systems, Inc.) were used as the counter and reference electrodes, respectively. The acquired impedance values were analyzed by using ZsimpWin software. Exosome concentration was determined with ELISA at 450 nm using the NanoDrop ND-1000 spectrophotometer (NanoDrop Technologies Inc., Wilmington, DE). All experiments were carried out at room temperature.

2.3. Colo 320 Cell Culture

Primary human colon cancer cell line (Colo 320, HTL95027, INTERLAB Cell Line Collection, Genova, Italy), was used to obtain exosomes. The Colo 320 cell line was cultured in RPMI-1640 (F-1213, Biochrom, Berlin, Germany) containing 10% fetal calf serum (FCS) (Capricorn Scientific, FBS-12B), 1% L-glutamine (Capricorn Scientific, GLN-B), and 1% penicillin-strept (Capricorn Scientific, PS-B). The cells were cultured at 37 °C in an incubator with 5% CO_2 (ESCO, CCL-170B-8). Morphological imaging of the cells was performed with an inverted microscope with phase contrast attachment (IX71, Olympus, Japan) in Figure 1. The morphology of the cells was shown to be a semi-adhesive structure.

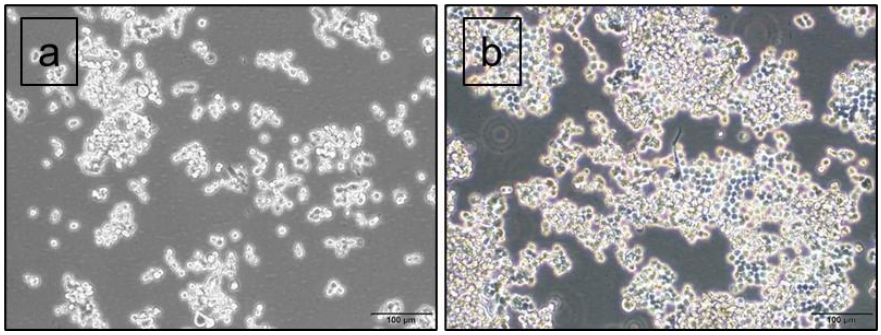

Figure 1. Colo 320 cell culture. Day 7 (a), day 14 (b) scale bars: 100 µm

2.4. Exosome Derivation

The miRCURY™ Exosome Isolation Kit (Exiqon 300102) was used for the exosome derivation. First, the cell culture condition media of Colo 320 were collected and centrifuged at 3200 g to get rid of the cell debris. After centrifugation, the supernatant was transferred to

another tube, and 4 ml of precipitation buffer was added and mixed. Then the samples were incubated for 60 min at 4 °C. Following the incubation, centrifugation was performed at 3200 g at 20 °C. Then the supernatant was removed, the pellet respined for 5 sec and the existing supernatant was discarded.

2.5. Exosome particle determination with ELISA

The exosome particle levels in the sample were measured spectrophotometrically by using a commercial assay kit, according to the manufacturer's instructions (ExoELISA-ULTRA Complete Kit (CD63 Detection), System Biosciences, CA, USA). Briefly, the various concentrations of standard proteins and exosome samples were added to the microtiter plate, after the commercially purchased standard proteins were thawed on ice. Then, the microtiter plate was covered with parafilm and incubated at 37 °C for 1 hour by gentle mixing. CD63 primary antibody was applied to each well and incubated at room temperature. A secondary antibody was added to each well in a blocking buffer and incubated for 1 hour. For each incubation step, the wells were washed with the buffer solution. After the samples were incubated with super-sensitive TMB ELISA substrate for 5-15 minutes in a shaker, a stop buffer was applied, and reading was performed at 450 nm in the ELISA reader.

2.6. Antibody modification of gold electrode

Firstly, a carboxylic acid decoration was obtained on a gold electrode surface with Au-S interaction after the treatment of MUA. For this purpose, the electrodes were immersed in 1 mM of MUA solution and then allowed to stir overnight at room temperature in the dark. After washing with ethanol to remove unbound MUA, the electrodes were treated with 0.4 M EDC.HCl and 0.1 M NHS for 1 hour to activate the carboxylic acid groups. After the process was completed, each electrode was incubated with 0.5 nM anti-CD63 for 2 hours at 4 ^{o}C. Then, the gold electrodes were washed with 1 ml of PBS 7.4. To prevent non-specific binding on the transducer surface of unmodified carboxylic acid groups, a final incubation was utilized in 0.1% BSA solution. After the modification steps, cyclic voltammetry (CV) and EIS measurements of anti-CD63 modified electrodes were recorded against the various concentrations of Colo 320 exosomes.

2.7. Exosome detection with EIS

We present an exosome biosensor based on a biological reaction between anti-CD63 antibody and CD63 exosome surface antigen. Since the Faradaic method was preferred in the measurements, 1 mM of $K_3[Fe(CN)_6]$ and $K_4[Fe(CN)_6]$ were used as the redox probe in PBS solution. After electrochemical measurements were obtained on antibody-modified electrodes, they were washed with pH 7.4 PBS buffer solution to have a free redox probe. Then, each

electrode was incubated with 250 µl exosome samples in the concentrations of 4.0×10^{12}, 1.2×10^{13}, 2.0×10^{13}, 2.8×10^{13}, 3.6×10^{13} exosome particles μL^{-1} at room temperature for 30 minutes as a moderate period. Electrochemical impedance spectroscopy results were evaluated in the form of '*relative response*' (RR_n) associated with an increasing amount of analyte to evaluate the biosensor system. RR_n is defined by:

$$RR_n^f = \left[RR_{Ex}^f - RR_{Ab}^f\right) / RR_{Ab}^f\right]$$

where RR_{Ab} was the response, when only antibody was attached at the transducer surface, i.e. no analyte at the surface, RR_{Ex} was the response received after incubation with the same frequency, *f,* different concentrations of exosome. By choosing the relative response method in the evaluation of real impedance analysis on the electrode surface, possible differences that may occur on the electrode surface were prevented.

The values of different electrical parameters have been extracted from experimental data with the help of ZsimpWin software. Validation of the data was provided with the chi-squared (χ^2) test. Relative change of chi-squared has been found less than 1×10^{-5} [45].

2.8. Curve Fitting

Since the concentration values of our samples were quite huge, we performed the *polyfit* command with the scaling option in MATLAB software to obtain the correct coefficients in the quadratic and cubic models for the calibration curve.

3. RESULTS AND DISCUSSION

3.1. Device Fabrication

The gold electrodes had two basic elements: the first one was the MUA monolayer, and the other was anti-CD63 used as an exosome bioreceptor. The MUA monolayer was attached to the gold electrode by an Au-S bond. Covalent immobilization of anti-CD63 to -COOH functional transducer was carried out with EDC/NHS coupling agents. Sensitivity as one of the most important factors in biosensor design was provided with anti-CD63 to capture and determine the exosome. In this case, the electrode was immersed into the sample, then exosomes were captured by antibodies specific to the CD63 surface antigen. Immobilization process was optimized with EIS which can provide information about R_{CT} changes on the electrode surface. Film formation (MUA) and analyte-specific antibody attachment via carbodiimide/succinimide chemistry was associated with an expected increase in charge transfer resistance, R_{CT}, from 10.9 ±0.4 kΩ (RSD%, 3.95%, n=3) to 30.1±3.3 kΩ (RSD %, 11%, n=3) for bare gold electrode and anti-CD63 modified electrode, respectively. Consequently, a prepared 4.00×10^{12} exosome particles μL^{-1} Colo 320 exosomes solution yielded in R_{CT} 39.5±0.3 kΩ (RSD %, 0.67%, n=3). The Nyquist plot of the biosensor system designed for exosome detection is shown in Figure 2a. In this graph, the data obtained at each

modification step were compared with simulated ones according to the R(C(RW)) equivalent circuit model. Moreover, Bode diagrams of the bare gold electrode, MUA, anti-CD63 and Colo 320 exosome modified gold electrode matrices and the frequency regions in the certain parts of the equivalent circuit were presented in Figure 2b.

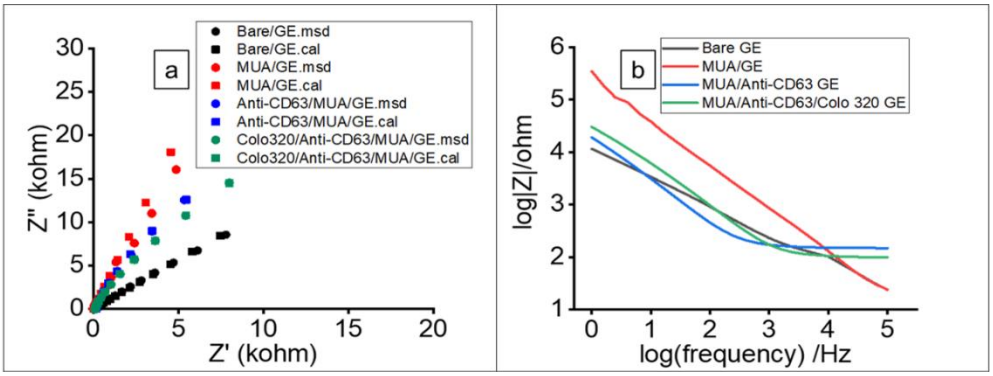

Figure 2. Nyquist plot (a) with measured (●) and simulated (■) data points and Bode Plot (b) of the bare, MUA, anti-CD63 and Colo 320 exosome (4.00×10^{12} exosome particles μL^{-1}) modified gold electrode in 1mM $K_3[Fe(CN)_6]/K_4[Fe(CN)_6]$/ PBS 7.4

CV measurements were taken after the modification process of the gold electrode and are indicated in Figure 3. According to these results, the current through the gold electrode was partially decreased by both anti-CD63 and exosome modification. No significant difference was observed in the different exosome concentrations applied.

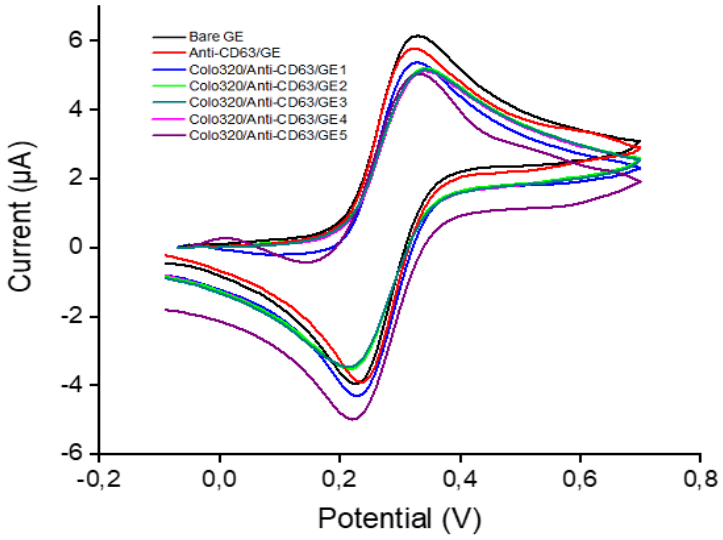

Figure 3. CV of electrodes with different modifications in solution of 1 mM $Fe(CN)_6^{3-/4-}$ in 0.1 M KCl, from Colo320/AntiCD63/GE1 to Colo320/AntiCD63/GE5 represent 4.00×10^{12}, 1.20×10^{13}, 2.00×10^{13}, 2.80×10^{13} and 3.60×10^{13} exosome particles μL^{-1}, respectively

3.2. Impedimetric Detection of Colo 320 Exosomes at Au/MUA/Anti-CD63

The Bode diagram was obtained as a function of the impedance output via the frequency of the applied potential. In all impedance measurements, the logarithmic value of the real impedance (log |Z|/ohm), which is the Bode Diagram output, was taken as a basis and indicated in Table 2. In addition, the Bode diagram in which the real impedance data of each electrode is obtained before and after different concentrations of exosome incubation is shown in Figure 4a. The *RR* values were calculated with the data obtained from this graph to be used in the calibration curve and were shown in Figure 4b.

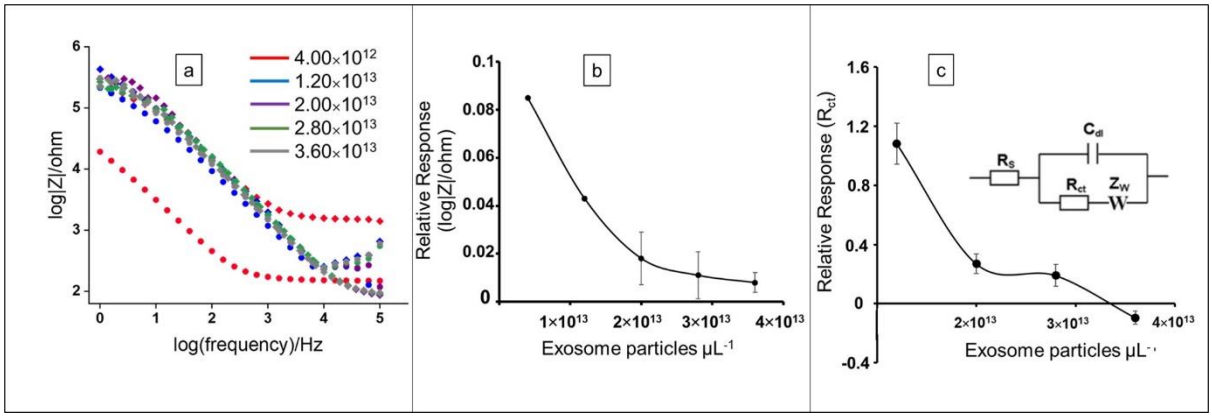

Figure 4. Bode diagram of the sensor before (●) and after (♦) applying the exosome at different concentrations (particles mL^{-1}) and Relative responses of real impedance at 100 Hz (b) and R_{ct} (c) by Randles Circuit Model. Error bars were generated from triplicate repeats across three independent electrodes.

Table 2. Relative responses for Colo 320 samples of various concentrations at *f*=100 Hz

Concentration (exosome particles/µl)	Signal (log|Z|/ohm)
4.00×10^{12}	0.0847
1.20×10^{13}	0.0429
2.00×10^{13}	0.0183
2.80×10^{13}	0.0112
3.60×10^{13}	0.0084

Three situations contribute to the electrical properties of the biosensor: *(i)* double layer effect arising from charged particles at the electrode surface, *(ii)* charge transfer between biomolecules and the electrode, *(iii)* diffusion component of the electroactive species to the electrode surface. After the exosome as a charged particle was bound onto the electrode, a double-layer effect was arisen by the applied potential at an impedimetric measurement. The decrease of relative response with the increase of the concentration of analytes indicated a better electron transfer for the ferrocyanide/ferricyanide redox couple [46,47]. Since the

antibodies that are responsible for exosome capture on the electrode surface interact with the target biomolecule, this behavior creates a charge perturbation [48,49]. Therefore, the decrease in the impedance can be interpreted as a result of the increase in biomolecule concentration [50,51]. We also calculated the charge transfer resistance (R_{CT}) and standard deviations corresponding to each concentration using the R(C(RW)) equivalent circuit model as indicated in Figure 4c.

3.3. Study of Calibration Curves

The analysis of the degree of relationship of the dependent variable with one or more independent variables, in other words 'regression', is the process of determining the model that best fits the curve formed by the data set. In regression, the best curve is expected to be as close as possible to the data points. Seemingly, a calibration curve with a calibration coefficient (R^2) greater than 0.9900 acquires more accurate results [52].

Needless to say, it is quite important to choose the best curve-fitting model for the data points to provide the most reliable results. If there is a linear relationship between the variables, namely, if the values of one variable are directly proportional to the other variable's values in a given range, then linear regression fits the best and generates very accurate results for this case. Particularly, in our case, a calibration curve based on the concentration versus signal is usually constructed by the linear model $y=mx+b$. Here, the concentration and signal are symbolized as x and y, respectively, and m refers to the slope. As mentioned above, if we fit a linear function to the data obtained as a result of our experiments, with the absolute value of the slope of the calibration curve in Figure 5A, we obtain the function.

$$y = -2 \times 10^{-15}\text{x} + 0.0792 \qquad Eq.1$$

The experimental signal results were compared with the signal results obtained by the linear function in Eq. 1 and the standard deviation was calculated for each concentration as $s = 0.01517$.

Moreover, we calculated $LOD\ as\ 2.50 \times 10^{13}\ exosome\ particles\ \mu L^{-1}$ by the Eq.2. The calculation method for the LOQ is again based on the standard deviation of the response and the slope of the calibration curve as stated in Eq. 3. The LOQ is also calculated for all functions whose LOD calculations are made and shown in Table 3.

$$LOD = \frac{\left(3.3\ x\ Standard\ Deviation\ of\ the\ Intersections\ of\ the\ Calibration\ Curve\right)}{(Slope\ of\ the\ Calibration\ Curve)} \qquad Eq.2$$

$$LOQ = \frac{\left(10\ x\ Standard\ Deviation\ of\ the\ Intersections\ of\ the\ Calibration\ Curve\right)}{(Slope\ of\ the\ Calibration\ Curve)} \qquad Eq.3$$

LOD and LOQ calculations were made for the determination method developed using the slope of function Eq. 2 and Eq. 3, respectively. However, since the slope calculation of nonlinear functions is complex, there is a restriction to use Eq. 2 and Eq. 3, directly. At this point, when the slope is calculated in the exponential function, second- and third-degree polynomial models, the equations mentioned become useful.

Due to the complex nature of biological measurements, it may not always be possible to observe the linear response. Hayashi et al. presented a proposal for the limit of detection and range of quantitation in nonlinear calibration curve for competitive ELISA, and an uncertainty equation was derived based on the possible error sources [53,54]. Analogously, a linear calibration curve was not suitable to fit perfectly to obtained data in our experiments as it can be observed from the calibration coefficient R^2=0.8351, which is quite less than 0.9900. Therefore, to increase the accuracy of our results (and R^2), we aimed to fit other possible curves by nonlinear regression to the data. At this point, we considered the best exponential curve of the form $y=ce^{Ax}$, quadratic and cubic polynomial models. Then, the experimental signals were compared with the signals obtained theoretically by the exponential function by Eq. 4 in Figure 5B.

$$P_1(\mathrm{x}) = ce^{Ax} = 0.1016e^{-7E-14x} \qquad Eq.4$$

For the determination of LOD, the standard deviation was calculated for the best exponential curve by formula Eq. 2 as $s = 0.00592$.

In literature, the slope of a nonlinear graph, *m*, used in the calculation of LOD could be utilized as the maximum of the absolute slope from the value of the curves [55,56]. The slope of the calibration curve drawn from the nonlinear equation of $y=ce^{Ax}$ became the greatest in two cases: a) At the endpoints of the derivative for the functions of (P_1'(4.00×10^{12}) and P_1'(3.60×10^{13})) b) The second derivative of the function was equal to zero or was undefined. Finally, we obtained two functions as below,

$$P_1{}'(\mathrm{x}) = -0.7112E - 14e^{-7E-14x},$$

$$P_1{}''(x) = 4.9784E - 28e^{-7E-14x}.$$

Due to the fact that the exponential functions are defined for all real numbers and are never zero, and their derivatives involve themselves; their derivatives are never zero as well. In particular, $P_1{}''(x)$ is never zero or undefined. Therefore, the point at the maximum absolute slope determined by evaluating the end points of (P_1'(4.00×10^{12}) and P_1'(3.60×10^{13})) as below:

$$|P_1{}'(4.00 \times 10^{12})| = 5.3751E - 15\ (max)$$

$$|P_1{}'(3.60 \times 10^{13})| = 5.7223E - 16.$$

Moreover, from Eq. 2

$$LOD = 3.64 \times 10^{12} exosome\ particles\ \mu L^{-1}.$$

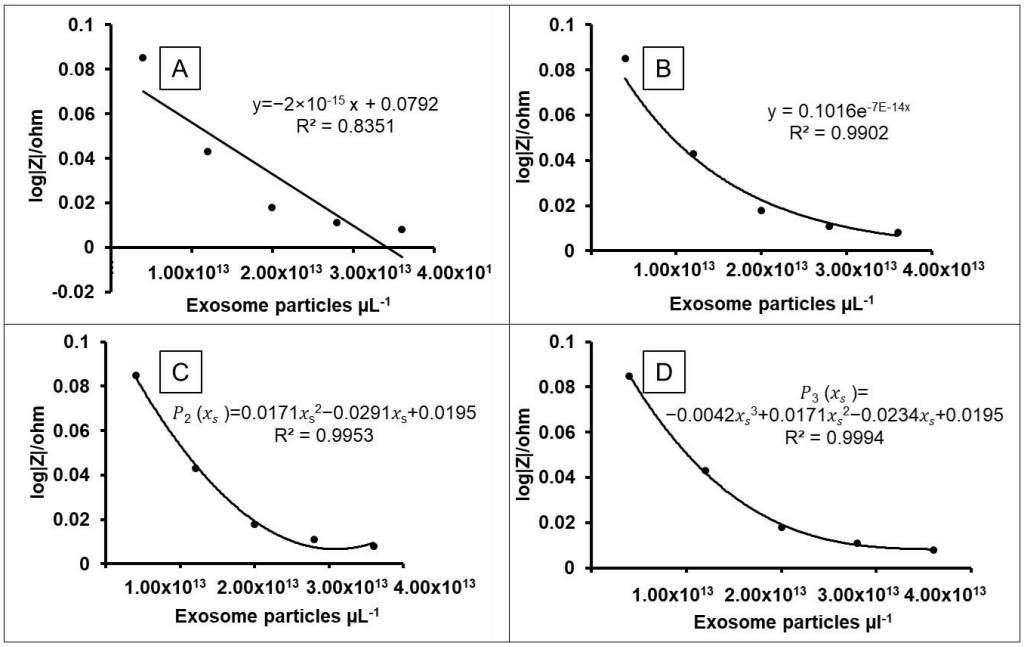

Figure 5. Calibration curves for Colo 320 cell lines, acquired by first, second, and third-degree polynomial models, and exponential function model

Although the obtained regression value of 0.9902 was close to the limit value of 0.9900, we considered another nonlinear equation to fit the calibration curve to obtain more accurate results.

A correct polynomial model might be determined by using the number of bends in the curve, and the number of bends, *n*, in a calibration graph is critical to determine the plot of a polynomial function and its derivation to be LOD and LOQ. So, the best fitting method is generally found as $(n+1)^{th}$ degree of polynomial function [57] i.e. quadratic polynomial model for one bend, while cubic polynomial model two bends. However, the use of a complex model serves a difficulty to observe the concentration and signal relation compared to one of a linear function. Since we supposed one bend in the data of our study, we fitted the quadratic term to the nonlinear model in Fig. 5C. Since we are dealing with huge numbers for the concentration, unlike the previous two cases, in the construction of the best quadratic polynomial (and cubic polynomial, later on) we encountered some problems with finding the coefficients. To overcome this trouble, we used the command *polyfit* with *scaling* our values in software MATLAB and ended up with the following (scaled) polynomial function:

$$P_2(x_s) = 0.0171x_s{}^2 - 0.0291x_s + 0.0195,$$

where the scaled value of *x* is calculated by $x_s = \frac{x-2\times10^{13}}{1.2649\times10^{13}}$.

Now, the standard deviation used in the determination of LOD was calculated from the best parabola as $s = 0.00222$. Moreover, the slope of the calibration curve was calculated as mentioned in the previous model. So, we obtained:

$$P_2{}'(x_s) = 7.9058 \times 10^{-14}(0.0342\, x_s - 0.0291),$$

$$P_2{}''(x_s) = \frac{0.0342}{(1.2649 \times 10^{13})^2}.$$

Since the second derivative was a nonzero constant, the greatest absolute slope occurred only at the end points of our interval which are the highest and lowest concentration values. Thus, the greatest absolute slope value was obtained for $P_2{}'(4.00{\times}10^{12})$ as follows:

$$|P_2{}'(4.00 \times 10^{12})| = 5.721 \times 10^{-15}\ (max)$$

$$|P_2{}'(3.60 \times 10^{13})| = 1.119 \times 10^{-15}.$$

Moreover, by Eq. 3

$$LOD = 1.28 \times 10^{12}\ exosome\ particles\ \mu L^{-1}.$$

In the quadratic polynomial model, R^2 was found as 0.9953, which is a more reasonable value compared to the previous models, yet we thought a higher degree polynomial model would give a better fitting and so the cubic polynomial model was performed by supposing two bends in the calibration curve. Lastly, we fitted the best cubic polynomial function for the calibration curve in Figure 5D, and as mentioned above, the *polyfit* command with scaling option in MATLAB showed the best cubic polynomial function

$$P_3(x_s) = -0.0042{x_s}^3 + 0.0171{x_s}^2 - 0.0234x_s + 0.0195,$$

where the scaled value of x was calculated by $x_s = \frac{x - 2{\times}10^{13}}{1.2649{\times}10^{13}}$.

The calibration coefficient of this cubic polynomial function was R^2 = 0.9994, indicating almost perfect regression for our data. For the calculation of LOD, the standard deviation was calculated as $s = 0.000811$. Moreover, we obtained the following functions,

$$P_3{}'(x_s) = 7.9058 \times 10^{-14} \times (-0.0126{x_s}^2 + 0.0342x_s - 0.0234),$$

$$P_3{}''(x_s) = 6.2501 \times 10^{-27} \times (-0.0252x_s + 0.0342).$$

Thus, $P_3{}''(x_s)$ equals to zero when

$$x_s = 1.3571, or\ x = 3.7167 \times 10^{13}.$$

Obviously, this value was out of the interval [$4.00{\times}10^{12}$, $3.60{\times}10^{13}$] for x values, hence $P_3{}'(x_s)$ can not be maximum slope at this point. Therefore, we only consider the following slope values at the end points of the interval:

$$|P_3{}'(4.00 \times 10^{12})| = 6.8638 \times 10^{-15}\ (max)$$

$$|P_3{}'(3.60 \times 10^{13})| = 2.3723 \times 10^{-17}.$$

Moreover, by Eq. 2, LOD was calculated as $3.90 \times 10^{11} exosome\ particles\ \mu l^{-1}$.

Mathematically, although nonlinear function models are much more suitable for nonlinear data compared to the linear function models, these models are rarely utilized in sensor applications. The results in Table 3 indicated that the calibration curve for the study of the determination of exosomes isolated from Colo 320 cell lines with the highest calibration coefficient (R^2=0.9994) and the lowest standard deviation (s=0.000811) was calculated from the cubic polynomial model.

Table 3. Comparing the curve-fitting effectiveness of the different methods

Equation Methods	Calibration Coefficient 'R²'	Standart Deviation 's'	LOD Exosomes /µL	LOQ Exosomes /µL
$y=-2\times10^{-15}x + 0.0795$	0.8351	0.01517	2.50×10^{13}	7.59×10^{13}
$y= P_1(x)=0.1032e^{-8E-14x}$	0.9902	0.00592	3.64×10^{12}	1.10×10^{13}
$y=P_2(x_s)=0.0171x_s^2-0.0291x_s+0.0195$	0.9953	0.00222	1.28×10^{12}	3.88×10^{12}
$y=P_3(x_s)=-0.0042x_s^3+0.0171x_s^2-0.0234x_s+0.0195$	0.9994	0.000811	3.90×10^{11}	1.18×10^{12}

4. CONCLUSION

We designed a biosensor for high concentration Colo 320 samples and developed a mathematical approach to finding the most reliable and accurate LOD value in calibration graph obtained from limited data and a narrow range of concentrations. We applied an electrochemical impedimetric analysis, which is one of the highly sensitive and label-free techniques for the quantification of Colo 320 exosomes in high concentrations. To determine the LOD and working range, four different mathematical models have been applied by using the concepts of curve fitting techniques for a linear function, exponential function, quadratic polynomial, and cubic polynomial. LOD value for exosome detection was 3.90×10^{11} particles μL^{-1} from third-order polynomial function as the lowest value of LOD. This paper serves as a powerful methodology to determine the exosome quantity in their high concentrations of media such as cell culture and to estimate LOD and LOQ values for a limited number of data groups that highly differ from the data in the calibration plot. This approach provides a fundamental concept for label-free electrochemical analysis of exosomes in their high concentrations.

Appendix A. Supplementary data

Acknowledgments

This research was founded by Gazi University Scientific Research Office (FCD-2021-7119). The authors would like to thank Ali Ugur Sazaklioglu (University of Turkish Aeronautical Association, Turkey) for his valuable comments and helpful suggestions for the improvement of this paper.

Declaration of Competing Interest

The authors declare that they have no known competing financial interests or personal relationships that could have appeared to influence the work reported in this paper.

REFERENCES

[1] B. F. Harry Heijnen, A. E. Schiel, R. Fijnheer, H. J. Geuze, and J. J. Sixma, Blood. 94 (1999) 3791.

[2] F. Momen-Heravi, L. Balaj, S. Alian, P. Y. Mantel, A. E. Halleck, A. J. Trachtenberg, C. E. Soria, S. Oquin, C. M. Bonebreak, E. Saracoglu, J. Skog, and W. P. Kuo, Biol. Chem. 394 (2013) 1253.

[3] J. van Deun, P. Mestdagh, R. Sormunen, V. Cocquyt, K. Vermaelen, J. Vandesompele, M. Bracke, O. de Wever, and A. Hendrix, J. Extracell. Vesicles. 3 (2014) 24858.

[4] S. Mathivanan, H. Ji, and R. J. Simpson, J. Proteomics. 73 (2010) 1907.

[5] N. Kastelowitz and H. Yin, ChemBioChem. 15 (2014) 923.

[6] C. Commisso, S. M. Davidson, R. G. Soydaner-Azeloglu, S. J. Parker, J. J. Kamphorst, S. Hackett, E. Grabocka, M. Nofal, J. A. Drebin, C. B. Thompson, J. D. Rabinowitz, C. M. Metallo, M. G. vander Heiden, and D. Bar-Sagi, Nature 497 (2013) 633.

[7] E. Delorme-Axford, R. B. Donker, J. F. Mouillet, T. Chu, A. Bayer, Y. Ouyang, T. Wang, D. B. Stolz, S. N. Sarkar, A. E. Morelli, Y. Sadovsky, and C. B. Coyne, Proc. Natl. Acad. Sci. USA. 110 (2013) 1248.

[8] O. P. B. Wiklander, J. Z. Nordin, A. O'Loughlin, Y. Gustafsson, G. Corso, I. Mäger, P. Vader, Y. Lee, H. Sork, Y. Seow, N. Heldring, L. Alvarez-Erviti, C. I. Edvard Smith, K. le Blanc, P. Macchiarini, P. Jungebluth, M. J. A. Wood, and S. el Andaloussi, J. Extracell Vesicles 4 (2015) 1.

[9] C. Admyre, S. M. Johansson, K. R. Qazi, J.-J. Filén, R. Lahesmaa, M. Norman, E. P. A. Neve, A. Scheynius, and S. Gabrielsson, J. Immun. 179 (2007) 1969.

[10] A. Suetsugu, K. Honma, S. Saji, H. Moriwaki, T. Ochiya, and R. M. Hoffman, Adv. Drug Deliv Rev. 65 (2013) 383.

[11] R. J. Bryant, T. Pawlowski, J. W. F. Catto, G. Marsden, R. L. Vessella, B. Rhees, C. Kuslich, T. Visakorpi, and F. C. Hamdy, Br. J. Cancer. 106 (2012) 768.

[12] S. H. Jalalian, M. Ramezani, S. A. Jalalian, K. Abnous, and S. M. Taghdisi, Anal. Biochem. 571 (2019) 1.

[13] N. Cheng, D. Du, X. Wang, D. Liu, W. Xu, Y. Luo, and Y. Lin, Trends Biotechnol. 37 (2019) 1236.

[14] D. Maiolo, L. Paolini, G. di Noto, A. Zendrini, D. Berti, P. Bergese, and D. Ricotta, Ana.l Chem. 87 (2015) 4168.

[15] Y. Jiang, M. Shi, Y. Liu, S. Wan, C. Cui, L. Zhang, and W. Tan, Angew. Chem. Int. Ed. 56 (2017) 11916.

[16] Y. T. Kang, Y. J. Kim, J. Bu, Y. H. Cho, S. W. Han, and B. I. Moon, Nanoscale 9 (2017) 13495.
[17] P. Zhang, M. He, and Y. Zeng, Lab Chip. 16 (2016) 3033.
[18] A. A. I. Sina, R. Vaidyanathan, S. Dey, L. G. Carrascosa, M. J. A. Shiddiky, and M. Trau, Sci. Rep. 6 (2016) 1.
[19] S. Picciolini, A. Gualerzi, R. Vanna, A. Sguassero, F. Gramatica, M. Bedoni, M. Masserini, and C. Morasso, Anal. Chem. 90 (2018) 8873.
[20] Z. Weng, S. Zong, Y. Wang, N. Li, L. Li, J. Lu, Z. Wang, B. Chen, and Y. Cui, Nanoscale 10 (2018) 9053.
[21] A. K. Pulikkathodi, I. Sarangadharan, C. Y. Lo, P. H. Chen, C. C. Chen, and Y. L. Wang, Int. J. Mol. Sci. 19 (2018) 2213.
[22] O. Alkhamis, J. Canoura, H. Yu, Y. Liu, and Y. Xiao, TrAC, Trends Anal. Chem. 121 (2019) 115699.
[23] Q. Li, G. K. Tofaris, and J. J. Davis, Anal. Chem. 89 (2017) 3184.
[24] Y. Zhu, Y. An, R. Li, F. Zhang, Q. Wang, and P. He, J. Electroanal. Chem. 862 (2020) 113969.
[25] A. Bagheri Hashkavayi, B. S. Cha, E. S. Lee, S. Kim, and K. S. Park, Anal. Chem. 92 (2020) 12733.
[26] T. Kilic, A. T. D. S. Valinhas, I. Wall, P. Renaud, and S. Carrara, Sci. Rep. 8 (2018) 9402.
[27] E. B. Bahadir and M. K. Sezgintürk, Artif Cells Nanomed. Biotechnol. 44 (2016) 248.
[28] T. Bertok, L. Lorencova, E. Chocholova, E. Jane, A. Vikartovska, P. Kasak, and J. Tkac, ChemElectroChem. 6 (2019) 989.
[29] J. Huang, Z. Li, B. Y. Liaw, and J. Zhang, J. Power Sources 309 (2016) 82.
[30] E. Cheever and Y. Li, Int. J. Engng Ed. 21 (2005) 335.
[31] J. D. Taylor and W. Messner, Int. J. Robust Nonlinear Control. 24 (2014) 3196.
[32] A. Pavlov, N. van de Wouw, and H. Nijmeijer, in Proceedings of the IEEE Conference on Decision and Control (2006) 3765.
[33] B. Langford, W. Acton, C. Ammann, A. Valach, and E. Nemitz, Atmos. Meas. Tech. 8 (2015) 4197.
[34] J. Uhrovčík, Talanta 119 (2014) 178.
[35] R. N. Goyal, V. K. Gupta, M. Oyama, and N. Bachheti, Electrochem. Commun. 7 (2005) 803.
[36] M. Thompson, S. L. R. Ellison, and R. Wood, Pure Appl. Chem. 74 (2002) 835.
[37] 37.Appendix B to Part 136. US Environmental Protection Agency (2012).
[38] The Fitness for Purpose of Analytical Methods: A Laboratory Guide to Method Validation and Related Topics, Second Edition (2014).
[39] A. Shrivastava and V. Gupta, Chron. Young Sci. 2 (2011) 21.
[40] W. Zhou, S. Yang, L. Wang, H. Sheng, and Y. Deng, J. Sens. (2021).

[41] I. G. Thakkar, K. L. Lear, J. Vickers, B. C. Heinze, and K. F. Reardon, Lab Chip. 13 (2013) 4775.
[42] M. H. F. Meyer, M. Hartmann, H. J. Krause, G. Blankenstein, B. Mueller-Chorus, J. Oster, P. Miethe, and M. Keusgen, Biosens. Bioelectron. 22 (2007) 973.
[43] L. Mauko, B. Ogorevc, and B. Pihlar, Electroanalysis 21 (2009) 2535.
[44] A. Belay, T. Ruzgas, E. Cso, G. Moges, M. Tessema, T. Solomon, and L. Gorton, Anal. Chem. 69 (1997) 3471.
[45] R. Pradhan, A. Mitra, and S. Das, in TechSym 2011-Proceedings of the 2011 IEEE Students' Technology Symposium (2011) 275.
[46] W. J. Niu, R. H. Zhu, S. Cosnier, X. J. Zhang, and D. Shan, Anal. Chem. 87 (2015) 11150.
[47] S. Y. Deng, T. Zhang, D. Shan, X. Y. Wu, Y. Z. Dou, S. Cosnier, and X. J. Zhang, ACS Appl. Mater Interfaces 6 (2014) 21161.
[48] F. Lisdat and D. Schäfer, Anal. Bioanal. Chem. 391 (2008) 1555.
[49] M. Wang, L. Wang, G. Wang, X. Ji, Y. Bai, T. Li, S. Gong, and J. Li, Biosens. Bioelectron. 19 (2004) 575.
[50] A. S. Tanak, B. Jagannath, Y. Tamrakar, S. Muthukumar, and S. Prasad, Anal. Chim. Acta X 3 (2019) 100029.
[51] E. Katz and I. Willner, Electroanalysis 15 (2003) 913.
[52] M. Kazusaki, S. Ueda, N. Takeuchi, and Y. Ohgami, Chromatography 33 (2012) 65.
[53] Y. Hayashi, R. Matsuda, K. Ito, W. Nishimura, K. Imai, and M. Maeda, Anal. Sci. 21 (2005) 167.
[54] Y. Hayashi, R. Matsuda, T. Maitani, K. Imai, W. Nishimura, K. Ito, and M. Maeda, Anal. Chem. 76 (2004) 1295.
[55] Á. Lavín, J. de Vicente, M. Holgado, M. F. Laguna, R. Casquel, B. Santamaría, M. V. Maigler, A. L. Hernández, and Y. Ramírez, Sensors 18 (2018) 2038.
[56] E. Rozet, E. Ziemons, R. D. Marini, and P. Hubert, Anal. Chem. 85 (2013) 6327.
[57] J. Frost, How to Choose Between Linear and Nonlinear Regression (2013).